Technical Report Documentation Page

Form DOT-F-1700.7

CA(FY)(RPMD#) **Block 1 Report Number** *For reports compiled on research*	
4. Title and Subtitle A DYNAMICAL FRAMEWORK FOR INTEGRATED CORRIDOR MANAGEMENT	5. Report Date 01/11/2016 6. Performing Organization code
7. Authors Ketan Savla, University of Southern California	8. Performing Organization Report No.
9. Performing Organization Name and Address California Department of Transportation Division of Research & Innovation 1227 O St Sacramento, CA 95814	10. Work Unit Number 11. Contract or Grant No. 65A0533
12. Sponsoring Agency Name and Address California Department of Transportation Sacramento, C A 95819	13. Type of Report and Period Covered Final Report, 01/01-12/31/2015 14. Sponsoring Agency Code
15. Supplementary Notes	

16. Abstract

We develop analysis and control synthesis tools for dynamic traffic flow over networks. Our analysis relies on exploiting monotonicity properties of the dynamics, and on adapting relevant tools from stochastic queuing networks. We develop proportional policies for traffic signal control, which are decentralized, and minimalist in that they require information only about local queue lengths. Hence, they are advantageous in the immediate aftermath of traffic incidents that cause significant changes in turning ratios and flow capacities on the links. Using dynamic traffic assignment framework, we develop convex formulations to compute variable speed limit and ramp metering controls over control horizon to optimize objectives, such as total travel time, which can be cast as convex functions. We also provide adaptation and convergence guarantees for distributed optimization techniques for these computations. The results are illustrated in case studies developed for Los Angeles sub-network in PTV VISSIM.

17. Keywords Decentralized Traffic Signal Control, Variable Speed Limit Control, Ramp Metering Control, Distributed Computation	18. Distribution Statement No restrictions. This document is available to the public through the National Technical Information Service, Springfield, VA 22161
19. Security Classif. (of this report) Unclassified 20. Security Classif. (of this page) Unclassified	21. No. of Pages 35 22. Price

2 Disclaimer Statement

The contents of this report reflect the views of the author(s) who is (are) responsible for the facts and the accuracy of the data presented herein. The contents do not necessarily reflect the official views or policies of the STATE OF CALIFORNIA or the FEDERAL HIGHWAY ADMINISTRATION. This report does not constitute a standard, specification, or regulation.

The contents of this report reflect the views of the authors, who are responsible for the accuracy of the data and information presented herein. This document is disseminated under the sponsorship of the Department of Transportation, University Transportation Centers Program, the California Department of Transportation and the METRANS Transportation Center in the interest of information exchange. The U.S. Government, the California Department of Transportation, and the University of Southern California assume no liability for the contents or use thereof. The contents do not necessarily reflect the official views or policies of the State of California, USC, or the Department of Transportation. This report does not constitute a standard, specification, or regulation

A Dynamical Framework for Integrated Corridor Management

Final Report

Metrans Project 14-09

January 2016

Principal Investigator:

Ketan Savla
Sonny Astani Department of Civil & Environmental Engineering
3620 S. Vermont Avenue, KAP 254A , University of Southern California
Los Angeles, CA 90089-2531
Tel: 213-740-0670 Fax: 213-744-1426
ksavla@usc.edu

Contents

List of Figures

List of Tables

6 Disclosure Section

Not Applicable

7 Foreword, Preface and Acknowledgements

This research was performed in collaboration with P. Hosseini at the University of Southern California, and G. Nilsson, E. Lovisari and G. Como, all from Lund University, Sweden. The author thanks Poornima Sundaram and Mahesh Tandarpally for their help with the simulations, and the Integrated Media Systems Center at USC for providing us the loop detector data.

8 Introduction

In this project, our objective was to build a comprehensive dynamical framework for traffic flow over integrated freeway and arterial road networks, develop stability analysis tools for such a framework, and use these tools to design dynamic traffic signal control, variable speed limit and ramp metering policy to optimize system efficiency and resiliency, with provable guarantees. Our control framework builds upon emerging sensing and control architecture, often collectively referred to as *cyber-physical systems* in the recent literature. In this report, we present our results on (i) convex formulations for dynamic traffic assignment to compute optimal variable speed limit control and ramp metering control, (ii) adaptation and convergence guarantees for distributed optimization algorithms to compute these controls, (iii) stability analysis of proportionally fair traffic signal control policies; and (iv) case study for a Los Angeles sub-network developed in PTV VISSIM, to compare the performance of max pressure and proportionally fair traffic signal control policies in terms of throughput and average travel time. Our presentation in Section 9 is divided along these four topics. In the remainder of the current section, we contextualize our work in the context of prior work.

Dynamic Traffic Assignment (DTA), introduced in [1, 2], has attracted a large amount of attention by the transportation research community, and has become a standard framework for control of freeway networks (see [3] for an overview). We focus on System Optimum Dynamic Traffic Assignment (SO-DTA) that aims at minimizing a system-level cost function over a planning horizon, subject to realistic traffic dynamics, and the presence of variable speed limits, ramp metering, and routing control.

The Cell Transmission Model (CTM), originally proposed in [4], is a compelling framework to simulate realistic traffic dynamics. Variable speed limits, ramp metering, and routing are the most widely studied forms of control for freeway networks. However, with very few exceptions (e.g., see [5]), these control strategies have not been incorporated in DTA formulations. The primary reason for not incorporating realistic traffic dynamics and control strategies in DTA is that finding numerical solutions for the resulting optimization problem is in general computationally expensive, and hence unsuitable for real-time applications. Convexity is a desirable property of optimization problems that facilitates their fast numerical solution, e.g., using readily available software tools such as `cvx` [6, 7].

Rapid advancements in traffic sensing technology have made it possible to use real-time traffic information in road traffic control. This has opened up the possibility of replacing traditional fixed-timing traffic signal controllers with adaptive controllers. Classical work on adaptive traffic signal controller does not provide any guarantees with respect to performance metrics of interest such as throughput, delay, and robustness to disruptions. Recently, well-known algorithms for routing in data networks, such as the back-pressure algorithm [8] and its throughput analysis, have been adapted to the traffic signal control setting, e.g., see [9, 10, 11]. However, these algorithms require the traffic signal controllers to have explicit knowledge about the turning ratios representing the route choice behavior of drivers, a requirement that may be impractical in many real-life applications.

While there has been growing interest recently in developing distributed traffic signal control for arterial road networks, distributed control or distributed algorithms to compute optimal control for freeway networks, with provable performance guarantees, has not attracted much attention.

9 Body of Report

Network flows [12] provide a compelling framework to model traffic flow over road networks. The static formulation consists of representing the road network by a directed graph, where the nodes correspond to traffic intersections and freeway junctions, whereas the directed links represent roads. Each link is associated with a flow capacity. External flow enters the network through a subset of nodes called origin nodes (or sources), and the flow leaves the network from a set of nodes called destination nodes (or sinks). A central problem in the network flow literature is the computation of the maximal set of inflows under which there exists a feasible flow distribution in the network, i.e., the one that satisfies link-wise capacity constraints and flow conservation at the nodes. Such feasible flows can be construed as equilibria for dynamical models for traffic flow over networks.

Dynamical models for traffic flow have been of intense research interest. The salient feature of these models is to describe the network state in terms of traffic density, and relate other traffic variables (i.e., flow and speed) through empirical relationships. One such relationship between flow and density is known as the *fundamental traffic diagram.* One of the well-known class of dynamical traffic models are the so-called hydrodynamic models, e.g., see [13], and their discretized counterparts, e.g., see [14]. Of particular relevance to this project is the cell transmission model [14]. These dynamical models have been fruitfully utilized for prediction and control purposes, primarily in the context of freeway traffic. While the static network flow formulation is obviously not well-suited for real-time traffic control, especially in the context of disruptions, its potential usage in establishing necessary and sufficient conditions for existence of equilibria for dynamical models has not been well studied yet.

We now describe the key research activities in the next four sub-sections: Sections 9.1 and 9.2 address control of freeway networks, whereas Sections 9.3 and Sections 9.4 address traffic signal control of arterial networks. Although the formalisms for these two networks, as presented here, are compatible with each other, their formal integration is topic of ongoing research, and will be published elsewhere.

9.1 Convexity and Robustness of Dynamic Traffic Assignment for Control of Freeway Networks

We describe the topology of the transportation network as a directed multi-graph $\mathcal{G} = (\mathcal{V}, \mathcal{E})$ with nodes representing junctions and links $i \in \mathcal{E}$ representing cells. The head and tail nodes of a cell i are denoted by τ_i and σ_i, respectively, so that the cell is directed from σ_i to τ_i. One particular node $w \in \mathcal{V}$ represents the external world, with cells i such that $\sigma_i = w$ representing on-ramps and cells i such that $\tau_i = w$ representing off-ramps. The sets of on-ramps and off-ramps will be denoted by $\mathcal{R}$ and $\mathcal{R}^o$, respectively. The network topology is typically illustrated by omitting such external node w and letting on-ramps have no tail node and off-ramps have no head node. (See Figure 1.) We will use the notation

$$\mathcal{A} = \{(i, j) \in \mathcal{E} \times \mathcal{E} : \tau_i = \sigma_j \neq w\}$$

for the set of all pairs of adjacent (consecutive) cells.

The dynamic state of the network is described by a time-varying vector $x(t) \in \mathcal{R}^{\mathcal{E}}$ whose entries $x_i(t)$ represent the mass (or traffic volume) in the cells $i \in \mathcal{E}$ at time t. The inputs of the network are the inflows $\lambda_i(t) \geq 0$ at the on-ramps $i \in \mathcal{R}$. Conventionally, we set $\lambda_i(t) \equiv 0$ for all non on-ramp cells $i \in \mathcal{E} \setminus \mathcal{R}$, and stack up all the inflows in a vector $\lambda(t) \in \mathcal{R}^{\mathcal{E}}$. The physical constraints are captured by the demand functions $d_i(x_i)$ and the supply functions $s_i(x_i)$, returning the maximum possible outflow from cells $i \in \mathcal{E}$ and the maximum possible inflow in the

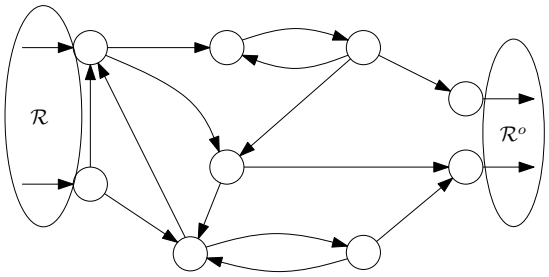

Figure 1: A multi-origin multi-destination cyclic network.

non on-ramp cells $i \in \mathcal{E} \setminus \mathcal{R}$, respectively, as a function of the current mass x_i. Conventionally, we put $s_i(x_i) \equiv +\infty$ at all on-ramps $i \in \mathcal{R}$. The demand functions are assumed to be continuous, non-decreasing, and such that $d_i(0) = 0$, while the supply functions are assumed to be continuous, non-increasing, and such that $s_i(0) > 0$, with $x_i^{\text{jam}} = \inf\{x_i > 0 : s_i(x_i) = 0\}$ denoting cell i's jam mass. Throughout, we focus on the case where all demand and supply functions are concave in their argument, which includes the common case of piecewise affine functions.

When formulating the DTA problems we will assume to be given an initial value $x_i^0 \geq 0$ on every cell $i \in \mathcal{E}$ and aim at minimizing the integral of a running cost $\psi(x)$ which is a function of the entire vector of mass x. We will assume that the running cost function $\psi(x)$ is convex in x, nondecreasing in each entry x_i, and such that $\psi(0) = 0$. A particularly relevant special case is when the cost function is separable, i.e., when

$$\psi(x) = \sum_{i \in \mathcal{E}} \psi_i(x_i)\,, \tag{1}$$

for convex non-decreasing costs $\psi_i(x_i)$ of the mass on the single cells $i \in \mathcal{E}$, with $\psi_i(0) = 0$. We will use the following optimization variables, all function of time: x_i, y_i, and z_i stand, respectively, for the mass on, the inflow in, and the outflow from, cell $i \in \mathcal{E}$; f_{ij} stands for the flow between two contiguous cells $i, j \in \mathcal{E}$ such that $\sigma_j = \tau_i$; and μ_i is the the out-flow from an off-ramp $i \in \mathcal{R}^o$ that leaves the network. Let $T > 0$ be the given time horizon.

We first introduce the basic version of the system optimum dynamic network traffic assignment (SO-DTA) problem that can be formulated as follows

$$\min \int_0^T \psi(x(t))\mathrm{d}t \tag{2}$$

such that,

$$x_i(0) = x_i^0\,, \qquad i \in \mathcal{E}\,, \tag{3}$$

and for all $t \in [0, T]$,

$$\dot{x}_i = y_i - z_i\,, \qquad i \in \mathcal{E}\,, \tag{4}$$

$$y_i = \lambda_i + \sum_{j \in \mathcal{E}} f_{ji}\,, \qquad z_i = \mu_i + \sum_{j \in \mathcal{E}} f_{ij}\,, \qquad i \in \mathcal{E}\,, \tag{5}$$

$$\mu_i \geq 0\,, \quad f_{ij} \geq 0\,, \qquad i, j \in \mathcal{E}\,, \tag{6}$$

$$
\begin{aligned}
f_{ij} &= 0 \qquad (i,j) \in \mathcal{E} \times \mathcal{E} \setminus \mathcal{A}\,, \\
\mu_i &= 0 \qquad i \in \mathcal{E} \setminus \mathcal{R}^o\,,
\end{aligned} \tag{7}
$$

$$
y_i \leq s_i(x_i)\,, \qquad z_i \leq d_i(x_i)\,, \quad i \in \mathcal{E}\,. \tag{8}
$$

Equation (3) prescribes an initial value of the cell mass x_i. Equation (4) captures the dynamical constraints that are derived from the law of mass conservation: the time-derivative of the x_i on a cell equals the imbalance between its inflow y_i and its outflow z_i. Equation (5) models flow conservation: it states that the inflow y_i in a cell is the aggregate of the external inflow λ_i and the flows f_{ji} from other cells in the network and, symmetrically, the outflow z_i from a cell is the aggregate of the flows f_{ij} to other cells in the network and the outflow μ_i towards the external world. The inequalities in (6) enforce non-negativity of the cell-to-cell flows f_{ij} and of the external outflows μ_i. Observe that, together with (5) and non-negativity of the external inflows λ_i, equation (6) implies non-negativity of the cells' inflows y_i and outflows z_i as well. Equation (7) captures the network topology constraints: the latter require that flows f_{ij} within the network are possible only between contiguous cells ($\tau_i = \sigma_j \neq w$), and outflows μ_i towards the external world are possible only from the off-ramps. Finally, the inequalities in (8) capture the physical constraints on the cells: they guarantee that the total inflow y_i in a cell does not exceed the supply $s_i(x_i)$, and the total outflow z_i from a cell does not exceed the demand $d_i(x_i)$. Because of the assumption $d_i(0) = 0$ and non-negativity of the cell inflow y_i, equation (4) implies that the mass x_i remains nonnegative in time, on every cell $i \in \mathcal{E}$.

Let us consider an exogenous, possibly time-varying, routing matrix R, which is a nonnegative $\mathcal{E} \times \mathcal{E}$ matrix satisfying the network topology constraints

$$
R_{ij} = 0\,, \qquad (i,j) \in (\mathcal{E} \times \mathcal{E}) \setminus \mathcal{A}\,, \tag{9}
$$

and such that

$$
\sum_{j \in \mathcal{E}} R_{ij} = 1\,, \qquad i \in \mathcal{E} \setminus \mathcal{R}^o\,. \tag{10}
$$

The matrix R is to be interpreted as describing the drivers' route choices, with its entries R_{ij}, sometimes referred to as turning ratios, representing the fractions of flow leaving cell i that wants to go to cell j. Equation (10) then guarantees that all the outflow from the non off-ramp cells is split among other cells in the network, while equation (9) guarantees that the outflow from cell i is split among adjacent downstream cells only.

We will consider two routing-constrained DTA problems. The first one, to be referred as the partially constrained (PC) SO-DTA consists in solving the minimization (2) under the constraints (3)–(8) and the additional constraint

$$
f_{ij} \leq R_{ij} d_i(x_i) \qquad i,j \in \mathcal{E}\,. \tag{11}
$$

The inequality above requires the flow f_{ij} from a cell i to a cell j not to exceed a given fraction R_{ij} of the demand $d_i(x_i)$ on cell i. Intuitively, if we interpret $d_{ij}(x_i) = R_{ij} d_i(x_i)$ as the aggregate demand of vehicles on cell i that want to move from cell i towards cell j, then inequality (11) constrains the actual flow f_{ij} from i to j not to exceed such demand. Observe that (11) is a convex constraint so that the (PC) SO-DTA remains a convex program. Clearly, the feasible set of the PC-SO-DTA problem is contained in the one of the SO-DTA problem, which in turn implies that the cost of an optimal solution of the PC-SO-DTA problem is never smaller than the one of an optimal solution of the SO-DTA.

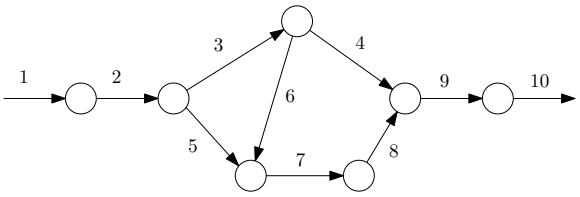

Figure 2: The network used in the numerical study.

The second routing-constrained DTA problem we propose, to be referred as the fully constrained (FC) SO-DTA consists in solving the minimization (2) under the constraints (3)–(8) and the additional constraint

$$f_{ij} = R_{ij} z_i \,, \qquad i \in \mathcal{E} \,. \tag{12}$$

The interpretation of (12) is that it forces the outflow from cell i to split exactly as prescribed by the routing matrix R, not only when it coincides with the demand $d_i(x_i)$ (as prescribed by (11)), but also when it is strictly smaller than that —e.g., when the supply constraint of one of the downstream links k (with $\sigma_k = \tau_i \neq w$) is satisfied with equality. Note that (12) and (8) jointly imply (11). Hence, the feasible set of the FC-SO-DTA problem —which is also convex since (12) is a linear constraint— is a subset of the feasible set of PC-SO-DTA and, *a fortiori*, of that of the SO-DTA problem. As an immediate consequence, we have the following inequalities

$$\Psi^* \leq \Psi^*_{PC} \leq \Psi^*_{FC} \,, \tag{13}$$

where Ψ^*, Ψ^*_{PC}, and Ψ^*_{FC} stand for the costs of an optimal solution to the SO-DTA, the PC-SO-DTA, and FC-SO-DTA, respectively.

Simulations: We solve all the SO-DTA variants in MatLab using the Convex Programming package `cvx` [6, 7]. We use the single-origin single-destination network described in [15] and shown in Figure 2 for our simulations. The scalability of the proposed methodologies to large networks is addressed via distributed algorithms in Section 9.2, where we show results for a large network 5. For implementation, we discretize the continuous formulation according to standard practices in Cell Transmission Models. Time is slotted with sampling time $\tau = 10$ seconds. In all the cells, demand and supply functions are piecewise affine:

$$d_i(x_i, t) = \min\{\frac{v_i x_i}{L_i}, C_i(t)\}$$
$$s_i(x_i, t) = \min\{\frac{w_i(x_i^{jam} - x_i)}{L_i}, C_i(t)\}$$

where v_i, w_i, $C_i(t)$, L_i and x_i^{jam} are the free-flow speed, the wave speed, the capacity (at time $t = 1, \ldots, n$), the length and the jam mass on cell i, respectively. The values of these parameters, along with number of lanes and length of cells, are specified in Table 1. The units of all parameters, as well as of inflows, provided below, are chosen in such a way that physical consistency is ensured. In addition, with the chosen parameters, a vehicle travels along an entire cell in exactly one time slot at maximum speed, which in the considered scenario is the free-flow speed v. Therefore, the Courant-Friedrichs-Lévy condition $\frac{\tau \max_i v_i}{\min_i L_i} \leq 1$, which is necessary for numerical stability, is satisfied.

Parameter	Value
Free-flow speed v_i, wave speed w_i	50 feet / sec
Length of cell L_i	500 feet
Capacity C_i	$6\ell_i$ veh/τ (except 4)
Number of lanes ℓ_i	2 for $i = 1, 2, 9, 10$; 1 otherwise
x^{jam}	$10\ell_i$ veh/ 500 feet

Table 1: Cell parameters.

Scheme	Cost
FIFO	281.6
SO-DTA	246
PC-SO-DTA	257.1
FC-SO-DTA	281.6

Table 2: Comparison between optimal cost for the three SO-DTA variants, and the cost for the system under FIFO rule, for the linear cost criterion.

Vehicles enter the network from cell 1 at rate $\lambda_1(t)$. We consider a setting in which[1] $\lambda_1(1) = 8$, $\lambda_1(2) = 16$, $\lambda_1(3) = 8$ and $\lambda_1(t) = 0$ for $t \geq 4$, with a time horizon of $T = 25$ steps, and in which the capacity in the cells is constant except on cell 4, where a bottleneck is simulated by setting $C_4(t) = 6$ veh/τ for $t \neq 5, 6, 7, 8$, $C_4(5) = C_4(6) = 0$ veh/τ, $C_4(7) = C_4(8) = 3$ veh/τ. Exogenous turning ratios are as follows: $R_{23} = 2/3$, $R_{25} = 1/3$ and $R_{34} = 2/3$, $R_{36} = 1/3$, the others being trivial.

For these values of inflow and link capacities, we computed optimal costs for all the three SO-DTA variants and the costs associated with a system evolving under FIFO policy with proportional merge rule. For brevity, we refer to the last model as FIFO. The initial condition for each case was $x(0) = 0$. The results for the total traffic volume cost $\Psi^{(1)}(x) = \sum_t \sum_{i \in \mathcal{E}} x_i(t)$ are reported in Table 2, whereas the results for the quadratic cost, $\Psi^{(2)}(x) = \sum_t \sum_{i \in \mathcal{E}} x_i^2(t)$, are reported in Table 3. The corresponding trajectories for volume of vehicles, $x_i(t)$, for a few representative cells are shown in Figures 3 and Figures 4 for linear and quadratic cost, respectively.

As expected, the SO-DTA, being the least constrained, gives the least cost, the FC-SO-DTA scheme gives the highest, and the PC-SO-DTA in between, for both linear and quadratic cost criteria. Moreover, again as expected, the optimal cost under any of the SO-DTA variant is no more than the cost under FIFO[2]. This favorable comparison between the optimal costs for the SO-DTA variants and the FIFO model serves as a motivation to investigate the feasibility of optimal SO-DTA solutions with respect to FIFO and other realistic traffic dynamics.

Control Design: The control inputs we consider for the FC-SO-DTA consist of a combination of ramp metering on the on-ramps and variable speed limits on the other cells. On the other hand, for the SO-DTA and the PC-SO-DTA, we also consider routing controls. We will assume that the

[1]Inflows are normalized by the onramp length as the dynamics involve the mass of vehicles.

[2]The results in Figures 3 and 4 also include results for the non-FIFO model, which is formally described in (21) and (22).

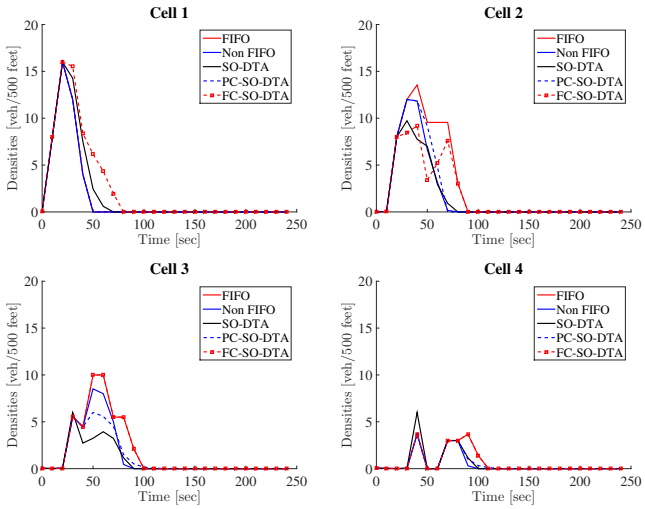

Figure 3: Trajectories of the number of vehicles on cells $1, 2, 3, 4$ for the system under FIFO rule and for the optimal solutions corresponding to the three variants of SO-DTA, for linear cost.

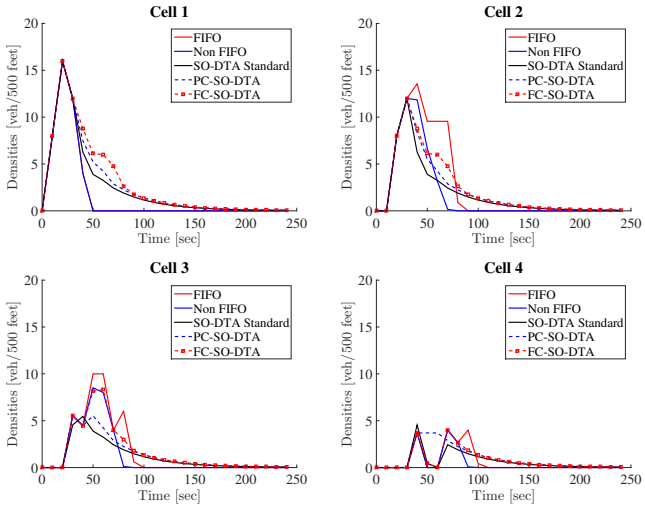

Figure 4: Trajectories of the number of vehicles on cells $1, 2, 3, 4$ for the system under FIFO rule and for the optimal solutions corresponding to the three SO-DTA variants, for quadratic cost.

Scheme	Cost
FIFO	1930.5
SO-DTA	1393.5
PC-SO-DTA	1537.5
FC-SO-DTA	1595.7

Table 3: Comparison between optimal cost for the three SO-DTA variants, and the cost for the system under FIFO rule, for the quadratic cost criterion.

controller has the ability to reduce the demand functions by setting controlled demand functions in the form

$$\overline{d}_i(x_i) = \alpha_i d_i(x_i)\,, \qquad i \in \mathcal{E} \setminus \mathcal{R} \tag{14}$$

$$\overline{d}_i(x_i) = \min\{d_i(x_i), c_i\}\,, \qquad i \in \mathcal{R} \tag{15}$$

where $\alpha_i \in [0,1]$ and $c_i \geq 0$ are control parameters. In the context of freeway networks, (14)–(15) can be realized through appropriate setting of speed limits and ramp metering. In particular, for linear uncontrolled demand functions $d_i(x_i) = v_i x_i$, formula (14) is equivalent to the modulation of the free-flow speed $\overline{v}_i = v_i \alpha_i$, where v_i could be interpreted as the maximum possible speed due to, e.g., safety considerations (Cf., e.g., [16]). On the other hand, (15) corresponds to metering the maximum outflow from the onramp, which is its demand $d_i(x_i)$, by imposing a maximum value c_i (Cf., e.g., [5]). The queue build-up due to the proposed speed limit control, or reduction of demand functions, is accommodated in our case due to unbounded queue capacities on on-ramps.

While control of the demand functions as above proves to be sufficient to ensure the feasibility of the solutions of the FC-SO-DTA with a given exogenous turning ratio matrix R, implementation of the solutions of the SO-DTA and of the PC-SO-DTA require additional actuation capabilities that allow for the design of a controlled turning ratio matrix $\overline{R}$ whose entries are nonnegative and satisfy the constraints (9) and (10). For consistency in notation, we will let $\overline{R} = R$ when discussing implementations of the FC-SO-DTA.

We now discuss the considered DNL models. For transportation systems, the term DNL generally refers to the modeling of the circular dependance between the network flow propagation and the link performance (cf., e.g., [17, Chapter 7]). In the specific framework considered here, such circular dependance is modeled by the differential equation (4), coupled with a functional dependance

$$f_{ij} = f_{ij}(x, \alpha, c, \overline{R})\,, \quad (i,j) \in \mathcal{A}\,,$$

$$\mu_k = \mu_k(x, \alpha)\,, \quad k \in \mathcal{R}^o$$

of the cell-to-cell flows and of the external outflows on the cell mass and the control parameters. In particular, we will focus on DNL models such that the external outflow from the off-ramps always coincides with their (controlled) demand, i.e.,

$$z_k = \mu_k = \overline{d}_k(x_k)\,, \qquad k \in \mathcal{R}^o\,; \tag{16}$$

and the outflow from every cell coincides with the controlled demand in the *free-flow region*, i.e.,

$$x \in \mathcal{F} \qquad \Longrightarrow \qquad z_i = \overline{d}_i(x_i)\,, \qquad \forall i \in \mathcal{E}\,, \tag{17}$$

where $\mathcal{F}$ denotes the free-flow region

$$\mathcal{F} := \left\{ x \in \mathbb{R}^{\mathcal{E}}_+ : \sum_{i \in \mathcal{E}} \overline{R}_{ij} \overline{d}_i(x_i) \leq s_j(x_j)\,, \forall j \in \mathcal{E} \right\}. \tag{18}$$

The considered DNL models differ for the way the cell-to-cell flows depend on the cell mass and on the control parameters in the congestion regime, i.e., when $\sum_{i \in \mathcal{E}} \overline{R}_{ij} \overline{d}_i(x_i) > s_j(x_j)$ for some cell $j \in \mathcal{E}$. Among the several possibilities, we will consider two specific cases:

1. the FIFO model

$$f_{ij}^{\mathrm{F}} = \overline{R}_{ij} z_i^F \,, \qquad z_i^F = \gamma_i^F \overline{d}_i(x_i) \,, \qquad (i,j) \in \mathcal{A} \,, \tag{19}$$

where for all $i \in \mathcal{E}$

$$\gamma_i^F = \sup \left\{ \gamma \in [0,1] : \gamma \cdot \max_{\substack{k \in \mathcal{E}: \\ (i,k) \in \mathcal{A}}} \sum_{h \in \mathcal{E}} \overline{R}_{hk} \overline{d}_h(x_h) \leq s_k(x_k) \right\} \tag{20}$$

2. and the non-FIFO model

$$f_{ij}^{\mathrm{N}} = \gamma_j^N \overline{R}_{ij} \overline{d}_i(x_i) \,, \qquad (i,j) \in \mathcal{A} \,, \tag{21}$$

where for all $j \in \mathcal{E}$

$$\gamma_j^N = \sup \left\{ \gamma \in [0,1] : \gamma \cdot \sum_{h \in \mathcal{E}} \overline{R}_{hj} \overline{d}_h(x_h) \leq s_j(x_j) \right\} \tag{22}$$

The FIFO DNL model (19)-(20) generalizes Daganzo's cell-transmission model [14] by extending it to the case where nodes (i.e., junctions) may have multiple incoming and outgoing links (cells). Since $f_{ij}^F = \overline{R}_{ij} z_i^F$ in every circumstances, the FIFO DNL is amenable to the modeling of multi-origin multi-destination transportation networks. However, as pointed out by some authors [18], it corresponds to a rather conservative behavioral model, in which not only do drivers never change their routing choice, thus blindly queuing up even in presence of alternative routes to the same destination, nor does it take into account presence of multiple lanes for multiple maneuvers at junctions. For example, a congested offramp on a freeway would slow down and possibly block the flow of vehicles on the main line, which is not always realistic.

On the other hand, the main difference of the non-FIFO model with respect to the FIFO one is that congestion in one of the outgoing cells does not influence the flow towards other outgoing cells. In the previous example, while the congested offramp forces vehicles that would like to take it to stop in the freeway, those that want to continue on the main line are free to do so, if the downstream supply of the main line is sufficient. In fact, the non-FIFO DNL model satisfies $f_{ij}^N = \overline{R}_{ij} z_i^N$ when $z_i^N = \overline{d}_i(x_i)$ (free-flow regime), whereas the actual turning ratios f_{ij}^N / z_i^N may deviate from the prescribed ones, namely, $\overline{R}_{ij}$, when $z_i^N < \overline{d}_i(x_i)$ (congested regime). As a consequence, the non-FIFO DNL model can be used for single-origin single-destination network (in which the actual path of a vehicle does not matter), but exhibits unrealistic behaviors in multi-origin multi-destination networks. A possibly more realistic model may involve a combination of the two DNL models —FIFO and non-FIFO— in which a fraction of drivers can change path, while another fraction cannot – for example, private cars can deviate from their path to chose a more convenient one, while buses or trucks have prescribed paths to follow.

To summarize, we consider DNL models that can all be written in the following form

$$\dot{x}_i(t) = \lambda_i(t) + g_i^M(x(t), \alpha(t), c(t), \overline{R}(t)) \,, \qquad i \in \mathcal{E} \,, \tag{23}$$

for all $t \in [0,T]$, where $\lambda_i(t)$ is the external inflow in cell i, $\alpha(t)$ is the vector of all demand control parameters, $c(t)$ is the vector of all ramp metering control parameters, and $\overline{R}(t)$ is the controlled

turning ratio matrix; the superscript M indices the specific model (i.e., $M = F$ for FIFO, $M = N$ for non-FIFO);

$$g_i^M(x,\alpha,c,\overline{R}) = \sum_{j\in\mathcal{E}} f_{ji}^M(x,\alpha,c,\overline{R}) - z_i^M,$$

$$z_i^M = \begin{cases} \sum_{j\in\mathcal{E}} f_{ij}^M(x,\alpha,c,\overline{R}) & i \in \mathcal{E}\setminus\mathcal{R}^o \\ \mu_i & i \in \mathcal{R}^o \end{cases} \tag{24}$$

and the outflows z_i^M satisfy (17).

We now address the issue of implementation of the optimal solutions to the SO-DTA, the PC-SO-DTA, and the FC-SO-DTA problems. Our result is summarized in the following.

(i) For any feasible solution $(x_i(t), y_i(t), z_i(t), \mu_i(t), f_{ij}(t))$ of the SO-DTA problem (3)-(8), set the demand controls $\alpha_i(t)$, ramp metering controls $c_i(t)$, and controlled turning ratio matrix $\overline{R}(t)$, for $t \in [0,T]$, as follows

$$\alpha_i(t) = \frac{z_i(t)}{d_i(x_i(t))}, \qquad \forall i \in \mathcal{E}\setminus\mathcal{R} \tag{25}$$

$$c_i(t) = z_i(t), \qquad \forall i \in \mathcal{R} \tag{26}$$

$$\overline{R}_{ij}(t) = \frac{f_{ij}(t)}{z_i(t)}, \qquad \forall i,j \in \mathcal{E} \tag{27}$$

with the convention that $\alpha_i(t) = 1$ if $z_i(t) = d_i(x_i(t)) = 0$ and that, if $z_i(t) = 0$, then $\overline{R}_{ij}(t) = |\{k \in \mathcal{E} : (i,k) \in \mathcal{A}\}|^{-1}$ for all $(i,j) \in \mathcal{A}$ and $R_{ij}(t) = 0$ for all $(i,j) \notin \mathcal{A}$. Then $x(t)$ coincides with the trajectory of the controlled DNL model (23)–(24).

Moreover, let $R(t)$, $t \in [0,T]$, be an exogenous turning ratio matrix. Then:

(ii) For any feasible solution $(x_i(t), y_i(t), z_i(t), \mu_i(t), f_{ij}(t))$ of the PC-SO-DTA problem (3)-(8) and (11), set the demand controls $\alpha_i(t)$ and controlled turning ratio matrix $\overline{R}(t)$, for $t \in [0,T]$, as in (25) and (27), respectively. Then, the following is satisfied:

$$\alpha_i \overline{R}_{ij} \le R_{ij}\,, \qquad i,j \in \mathcal{E}, i \notin \mathcal{R}\,. \tag{28}$$

and $x(t)$ coincides with the trajectory of the controlled DNL model (23)–(24).

(iii) For any feasible solution $(x_i(t), y_i(t), z_i(t), \mu_i(t), f_{ij}(t))$ of the FC-SO-DTA problem (3)-(8) and (12), set the demand controls $\alpha_i(t)$, for $t \in [0,T]$, as in (25), and let controlled turning ratio matrix $\overline{R}(t) = R(t)$ coincide with the uncontrolled one. Then, $x(t)$ coincides with the trajectory of the controlled DNL model (23)–(24).

Furthermore, in all the three cases (i)–(iii) above, the implemented trajectory is in the free-flow region for all $t \in [0,T]$.

Simulation results illustrating the utility of our control design, and sensitivity analysis with respect to perturbations in inflow λ, along with other details of the results described here, can be found in our related publication [19].

9.2 Distributed Computation of Optimal Equilibrium for Traffic Networks

We adopt the same framework as adopted in Section 9.1. However, we repeat a few key aspects here for the sake of completeness.

The dynamic state of the network is described by a time-varying vector $\rho(t) \in \mathcal{R}^{\mathcal{E}}$ whose entries $\rho_i(t)$ represent the densities in the cells $i \in \mathcal{E}$ at time t. The inputs of the network are the inflows $\lambda_i(t) \geq 0$ at the on-ramps $i \in \mathcal{R}$. Conventionally, we set $\lambda_i(t) \equiv 0$ for all non on-ramp cells $i \in \mathcal{E} \setminus \mathcal{R}$, and stack up all the inflows in a vector $\lambda(t) \in \mathcal{R}^{\mathcal{E}}$. The dynamical model is described by a system of ODEs:

$$\dot{\rho}_i = f_i^{\text{in}}(\rho) - f_i^{\text{out}}(\rho)\,, \qquad i \in \mathcal{E} \tag{29}$$

Here, $\rho_i \geq 0$ stands for the density on a cell i, $\rho \in \mathbb{R}_+^{\mathcal{E}}$ stands for the vector of all densities on the different cells, and $f_i^{\text{in}}(\rho)$ and $f_i^{\text{out}}(\rho)$ denote the inflow to and, respectively, the outflow from cell i. Following Daganzo's seminal work [4, 14], the physical characteristics of each cell i are captured by a demand function $d_i(\rho_i)$ and a supply function $s_i(\rho_i)$, representing upper bounds on the outflow from and, respectively, the inflow in cell i at time t, when the current density on it is ρ_i, i.e.,

$$f_i^{\text{in}}(\rho) \leq s_i(\rho_i)\,, \qquad f_i^{\text{out}}(\rho) \leq d_i(\rho_i)\,, \qquad i \in \mathcal{E}\,. \tag{30}$$

The *jam density* on cell i, namely, the maximum density allowed on i, is defined as $B_i := \sup\{\rho \geq 0 :\ s_i(\rho, t) > 0\}$. Observe that (30) implies that the set $\mathcal{S} := \prod_{i\in\mathcal{E}}[0, B_i]$ is invariant under the dynamics (29). The function $g_i(\rho_i) = \min\{d_i(\rho_i), s_i(\rho_i)\}$ is often interpreted as the *fundamental diagram* and $C_i := \max_{\rho_i \geq 0} g_i(\rho_i)$ as the *flow capacity* of cell i. A particularly relevant role in the applications has been played by the special case of linear demand functions $d_i(\rho_i) = v_i\rho_i$, where v_i is the *free-flow speed* and saturated affine supply functions $s_i(\rho_i) = \min\{S_i, w_i(B_i - \rho_i)\}$, where w_i is the wave-speed and S_i a supply saturation level. We will also use the convention that on all on-ramps $i \in \mathcal{R}$ the supply and jam density are infinite, i.e., $s_i(\,\cdot\,,\,\cdot\,) \equiv +\infty$ and $B_i = +\infty$. In contrast, we will assume that the jam density on every other cell is finite, i.e., $B_i < +\infty$ for all $i \in \mathcal{E} \setminus \mathcal{R}$.

The network topology described by the directed graph $\mathcal{G}$ induces natural constraints on the dynamics (29): flow is possible only between consecutive cells, i.e., from a cell i to a cell j such that $\tau_i = \sigma_j$. Specifically, we model the flow $f_{ij}(\rho)$, $(i,j) \in \bar{\mathcal{A}}$, as a continuous function of ρ, and let the inflow in and outflow from a cell i, respectively, satisfy the following for all $i \in \mathcal{E}$

$$f_i^{\text{in}}(\rho) = \lambda_i + \sum_{j\in\mathcal{E}_i^-} f_{ji}(\rho), \quad f_i^{\text{out}}(\rho) = \sum_{j\in\mathcal{E}_i^+} f_{ij}(\rho) \tag{31}$$

The actual form of the flow functions $f_{ij}(\rho)$ depends on a *turning preference matrix* $R \in \mathbb{R}^{\bar{\mathcal{A}}}$ satisfying, for all $i \in \mathcal{E}$ and $j \in \bar{\mathcal{E}}$, $R_{ij} \geq 0$, $\sum_{k\in\mathcal{E}_i^+} R_{ik} = 1$ and $R_{ij} = 0$ if $\tau_i \neq \sigma_j$. In particular, the flow functions have to satisfy the following natural constraints

$$\begin{aligned} &0 \leq f_{ij}(\rho) \leq R_{ij} d_i(\rho_i)\,, \qquad \forall (i,j) \in \mathcal{A} \\ &\lambda_i + \sum_{j\in\mathcal{E}_i^-} f_{ji}(\rho) \leq s_i(\rho_i)\,, \qquad \forall i \in \mathcal{E} \end{aligned} \tag{32}$$

and, for all $v \in \mathcal{V}$,

$$\begin{aligned} \sum_{j\in\mathcal{E}_i^-} R_{ji} d_j(\rho_j) \leq s_i(\rho_i) \quad \forall i \in \mathcal{E}_v^+ \\ \Longrightarrow f_{ji}(\rho) = R_{ji} d_j(\rho_j) \quad \forall j \in \mathcal{E}_v^- \end{aligned} \tag{33}$$

and the outflow from every off-ramp is equal to demand, i.e.,

$$\sum_{j\in\mathcal{E}_i^+} f_{ij}(\rho) = d_i(\rho_i), \quad i \in \mathcal{R}^o. \tag{34}$$

The constraints (32)–(34) do not uniquely characterize the value of the flow functions $f_{ij}(\rho)$ when $\sum_{j\in\mathcal{E}_i^-} R_{ji}d_j(\rho_j) > s_i(\rho_i)$. In this case, (32) only ensures that the total inflow in i does not exceed the supply of cell i, while specific allocation rules are needed to determine how much of such supply is allocated to the flows from the different cells $i \in \mathcal{E}_j^-$. We consider a non-First In First Out (non-FIFO) policy, according to which $f_{ij}(\rho) = \gamma_j R_{ij} d_i(\rho_i)$ for all $(i,j) \in \mathcal{A}$, where for all $j \in \mathcal{E}$, $\gamma_j = \sup\left\{\gamma \in [0,1] : \gamma \cdot \sum_{h\in\mathcal{E}} R_{hj} d_h(\rho_h) \le s_j(\rho_j)\right\}$.

The Optimal Equilibrium Selection Problem: For given λ, R, demand and supply functions on the links, existence and stability of equilibria for the dynamical model, described by (29)-(33) under non-FIFO policy has been studied in our previous work [20, 21]. Let $\mathcal{F}$ be the set of (ρ, f) that satisfy the following:

$$\begin{aligned}
\rho_i &\ge 0 && \forall\, i \in \mathcal{E} \\
f_{ij} &\ge 0 && \forall\, (i,j) \in \bar{\mathcal{A}} \\
\sum_{j\in\mathcal{E}_i^+} f_{ij} &= \lambda_i + \sum_{j\in\mathcal{E}_i^-} f_{ji} && \forall i \in \mathcal{E} \\
\lambda_i + \sum_{j\in\mathcal{E}_i^-} f_{ji} &\le s_i(\rho_i) && \forall i \in \mathcal{E} \\
\sum_{j\in\mathcal{E}_i^+} f_{ij} &\le d_i(\rho_i) && \forall i \in \mathcal{E}
\end{aligned} \tag{35}$$

One can easily check that $\mathcal{F}$ is a relaxation of the actual constraints imposed by the dynamics at equilibrium, as described by (29)-(34), and the non-FIFO policy. In our previous work [20], we showed that, for every $(\rho, f) \in \mathcal{F}$, one can design variable speed (to change demand functions on non on-ramp links), ramp metering (to change demand functions on on-ramps) and routing matrix R under which (ρ, f) is an equilibrium for the dynamical model under non-FIFO policy. Moreover, the set $\mathcal{F}$ is convex in (ρ, f). This motivates finding a point in $\mathcal{F}$ that is optimal with respect to a prescribed convex cost function. Accordingly, we consider the following problem:

$$\min_{(\rho,f)\in\mathcal{F}} \sum_{i\in\mathcal{E}} \psi_i(\rho_i) + \sum_{(i,j)\in\bar{\mathcal{A}}} \xi_{ij}(f_{ij}) \tag{36}$$

The primal and dual updates, corresponding to the Alternating Direction Method of Multipliers (ADMM), can be written in a concise form as follows:

For all $i \in \mathcal{E} \backslash \mathcal{R}^o$:

$$\begin{aligned}\begin{bmatrix} \bar{f}_i(k+1) \\ \rho_i(k+1) \end{bmatrix} = & \underset{(\bar{f}_i,\rho_i)\in\mathcal{D}_i}{\operatorname{argmin}} \ \psi_i(\rho_i) + \sum_{(i,j)\in\bar{\mathcal{A}}} \xi_{ij}(f_{ij}) \\ & + \frac{\alpha}{2} \sum_{j\in\mathcal{E}_i^+} \left(f_{ij} - f_{ij}(k) - \Delta_i(k) + y_i(k) - y_j(k)\right)^2 \\ & + \frac{\alpha}{2} \left(\sum_{j\in\mathcal{E}_i^+} f_{ij} - \sum_{j\in\mathcal{E}_i^+} f_{ij}(k) + \Delta_i(k) \right)^2 \end{aligned} \tag{37a}$$

For all $i \in \mathcal{R}^o$:

$$\begin{aligned}\begin{bmatrix} f_{ij}(k+1) \\ \rho_i(k+1) \end{bmatrix} = & \underset{(\bar{f}_i,\rho_i)\in\mathcal{D}_i}{\operatorname{argmin}} \ \psi_i(\rho_i) \\ & + \frac{\alpha}{2} \left(f_{ij} - f_{ij}(k) + \Delta_i(k) + y_i(k)\right)^2 \end{aligned} \tag{37b}$$

For all $i \in \mathcal{E}$:

$$\begin{aligned} \Delta_i(k+1) &= \frac{\sum_{j\in\mathcal{E}_i^+} f_{ij}(k+1) - \sum_{j\in\mathcal{E}_i^-} f_{ji}(k+1) - \lambda_i}{n_i + 1} \\ y_i(k+1) &= y_i(k) + \Delta_i(k+1) \end{aligned} \tag{37c}$$

The distributed setting for executing the iterations in (37) is as follows. Each link i is associated with a processing unit, which is responsible for updating $\{\bar{f}_i, \rho_i, y_i\}$ according to (37). During every iteration, the unit on link i communicates with its neighboring units twice as follows: after the primal update, unit i sends the most current values of $\bar{f}_i$ to the units on $\mathcal{E}_i^+$, and after the dual update, unit i sends the most current values of y_i to the units on $\mathcal{E}_i^-$. We assume synchronous operation between the processing units.

The following result gives sufficient conditions under which the iterates of (37) converge to an optimal solution of (36).

Let (ρ^*, f^*) be the solution to the optimal equilibrium selection problem in (36), and $(\rho(k), f(k))$ be the iterations in (37). If $\sum_{j\in\mathcal{E}_i^+} f_{ij}^* < C_i$ for all $i \in \mathcal{E}$, then $(\rho(k), f(k)) \to (\rho^*, f^*)$ as $k \to +\infty$.

The proof of this result, as well as the iterations for Newton's method inspired by the Accelerated Dual Descent method for network flow optimization from [22] can be found in our related publication [23].

Simulations: The ADMM and ADD based methods were implemented on the network illustrated in Fig 5, with supply and demand functions taken as $s_i(\rho_i) = 10 - \rho_i$ and $d_i(\rho_i) = \rho_i$ for all i. The inflows and outflows are set to be zero, except for the following components: $\lambda(1) = \lambda(12) = 1$, $\lambda(9) = 2$, and $\mu(27) = \mu(32) = 2$. The cost functions are chosen to be $\psi_i(\rho_i) = \rho_i^2$ for all i, and $\xi_{ij}(f_{ij}) = 0.2 f_{ij}^2$.

The simulation results for the ADMM method, as shown in Fig. 6, illustrate convergence of the primal variables. The simulation results for the ADD-based method in Fig. 7, show the improvements in the convergence rate with increasing truncation terms N in the approximations of the pseudo-inverse of the Hessian.

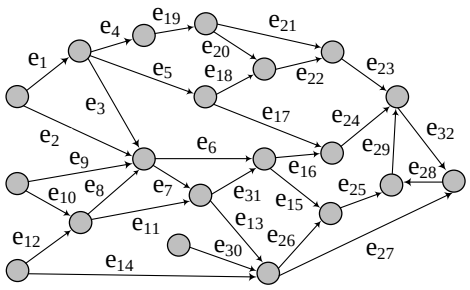

Figure 5: A directed cyclic network with 20 nodes and 32 links used in the simulations

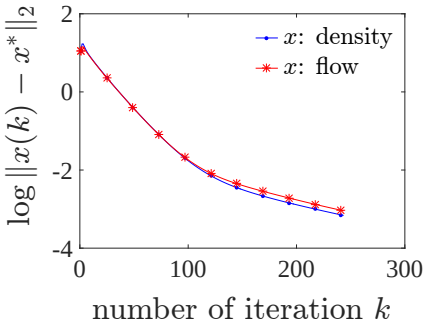

Figure 6: Convergence of the primal variables to their optimal values under ADMM.

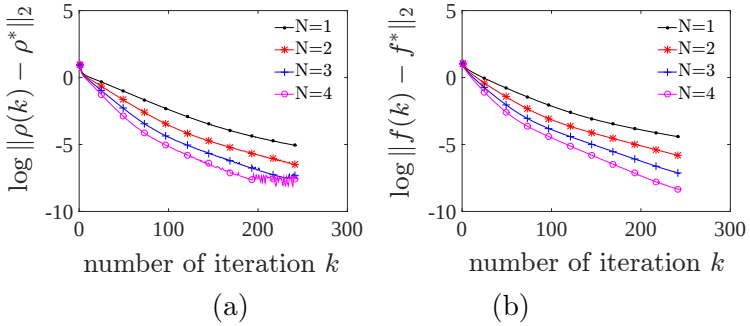

Figure 7: Convergence of link densities (a) and flow (b) to their optimal values under the ADD-based method for different number of truncation terms N.

9.3 Stability Analysis and Throughput Optimality of Proportionally Fair Traffic Signal Control Policies

In this section, we present our key results on stability analysis of proportionally fair controllers – further details can be found in our related publication [24].

We describe the topology of a urban traffic network as a capacitated directed graph $\mathcal{G} = (\mathcal{V}, \mathcal{E}, C)$, whose nodes $v \in \mathcal{V}$ represent junctions and whose links $i \in \mathcal{E}$ represent lanes, and where $C \in \mathcal{R}^{\mathcal{E}}$ is a vector whose entries $C_i > 0$ represent the flow capacities of the lanes $i \in \mathcal{E}$. Traffic flows among consecutive lanes according to a *routing matrix* $R \in \mathcal{R}_+^{\mathcal{E}\times\mathcal{E}}$ whose (i,j)-th entry R_{ij} —which will be referred to as a *turning ratio*— represents the fraction of flow out of lane i that joins lane j. Conservation of mass implies that $\sum_{j\in\mathcal{E}} R_{ij} \leq 1$ for all $i \in \mathcal{E}$, the quantity $1 - \sum_{j\in\mathcal{E}} R_{ij} \geq 0$ representing the fraction of flow out of lane i that leaves the network directly. In other words, the routing matrix R is sub-stochastic. Moreover, the natural topological constraints encoded in the graph $\mathcal{G}$ imply that $R_{ij} = 0$ if $\tau_i \neq \sigma_j$, i.e., $R_{ij} = 0$ whenever lane i does not end in the junction where lane j starts. We will refer to this property of the routing matrix R as being *adapted* to $\mathcal{G}$. Finally, we consider an *arrival vector* $\lambda \in \mathcal{R}_+^{\mathcal{E}}$, whose entries $\lambda_i \geq 0$ describe the external inflows on the lanes $i \in \mathcal{E}$.

In order to complete the description of the urban traffic network, we need to introduce the notion of *phases*. These are subsets of lanes that can be given green light simultaneously. We will thus identify every phase with a binary vector $p \in \{0,1\}^{\mathcal{E}}$ whose i-th entry p_i equals 1 if lane i receives green light during phase p and 0 otherwise. The set of all possible phases will be denoted by $\Psi \subseteq \{0,1\}^{\mathcal{E}}$.

We will then study continuous-time dynamics with state vector $\rho(t) \in \mathcal{R}_+^{\mathcal{E}}$ whose entries $\rho_i(t)$ denote the traffic volume on the lanes $i \in \mathcal{E}$. Such dynamics are of the form

$$\dot{\rho}_i = \lambda_i + \sum_{j\in\mathcal{E}} R_{ji} C_j h_j(\rho) - C_i h_i(\rho), \quad \forall i \in \mathcal{E}\,. \tag{38}$$

In equation (38) above, when $\rho_i > 0$, the term $h_i(\rho)$ represents the total fraction of time that lane i is given green light. This can be expressed as

$$h_i(\rho) = \sum_{p\in\Psi} \theta_p(\rho) p_i\,, \qquad \text{if } \rho_i > 0\,, \tag{39}$$

where $\theta_p(\rho)$ represents the fraction of time that phase p is activated. Here, $\theta(\rho)$ is a *green light (feedback) policy*: the domain of θ is $\mathcal{R}_+^{\mathcal{E}}$, while its range is the simplex $\mathcal{S}$ of probability vectors over the set of phases Ψ. In other terms, for all network states $\rho \in \mathcal{R}_+^{\mathcal{E}}$, $\theta(\rho)$ is a vector with nonnegative entries $\theta_p(\rho)$ indexed by the phases $p \in \Psi$, such that $\sum_{p\in\Psi} \theta_p(\rho) = 1$.

Observe that if an equilibrium ρ^* of the dynamical system (38) exists with all positive entries, it must satisfy

$$0 = \lambda_i + \sum_{j\in\mathcal{E}} R_{ji} C_j h_j(\rho^*) - C_i h_i(\rho^*),$$

which can be compactly written as

$$\lambda + (R^T - I)\mathrm{diag}\,(C)\, h(\rho^*) = 0,$$

or

$$h(\rho^*) = \mathrm{diag}\,(C)^{-1}\, a, \qquad a := (I - R^T)^{-1}\lambda\,. \tag{40}$$

This argument implies the following result.

If the dynamical system (38) admits an equilibrium ρ^* with all positive entries, then it must hold that

$$\operatorname{diag}(C)^{-1} a \in \operatorname{conv}(\Psi)\,, \tag{41}$$

where

$$a = (I - R^T)^{-1}\lambda\,. \tag{42}$$

We will focus on the case where $\operatorname{diag}(C)^{-1} a \in \operatorname{int}(\operatorname{conv}(\Psi))$ and study green light policies that admit (globally asymptotically) stable equilibria. We will consider sets of phases that model local constraints among the incoming lanes in each intersection $v \in \mathcal{V}$. Specifically, observe that the set of lanes can be partitioned as $\mathcal{E} = \cup_{v\in\mathcal{V}}\mathcal{E}_v$, where $\mathcal{E}_v$ stands for the set of lanes coming into junction v.

We will then focus on green light policies $\theta(\rho)$ that can be written as the concatenation of local policies $\theta^{(v)}(\rho^{(v)})$ —where $\rho^{(v)} = (\rho_i)_{i\in\mathcal{E}_v}$ is the vector of densities on the lanes coming into junction $v \in \mathcal{V}$— of the following form

$$\theta^{(v)}(\rho^{(v)}) \in \operatorname*{argmax}_{\theta\in\mathcal{S}_v} \sum_{i\in\mathcal{E}_v} \rho_i \log(\sum_{p\in\Psi_v} \theta_p p_i) + \kappa_v \log\theta_0\,, \tag{43}$$

where $\mathcal{S}_v$ is the simplex of probability vectors over Ψ_v and $\kappa_v > 0$ is the *zero phase weight*. The zero phase is introduced to capture the fact that under normal traffic demands, a fraction of the possible utilization is used to phase shifts.

From now on, with a slight abuse of notation, we will refer to

$$h^{(v)}(\rho^{(v)}) = \sum_{p\in\Psi_v} \theta_p^{(v)}(\rho^{(v)})p\,, \qquad \forall v \in \mathcal{V} \tag{44}$$

as the *maximizing green light policy*.

In this section we focus on the special case of phase sets that do not allow for multiphases, i.e., where every phase can prescribe green light to at most one lane incoming to a junction. Specifically, we assume that the local set of phases at every intersection is

$$\Psi_v = \{p \in \{0,1\}^{\mathcal{E}_v} : \sum_{e\in\mathcal{E}_v} p_e \le 1\}\,, \qquad \forall v \in \mathcal{V}. \tag{45}$$

In this case, the necessary condition for stability (41) takes the form

$$a_i \ge 0\,, \quad \forall i \in \mathcal{E}\,, \qquad \sum_{i\in\mathcal{E}_v} \frac{a_i}{C_i} < 1\,, \qquad \forall v \in \mathcal{V}\,.$$

Moreover, the green light policy can be expressed explicitly as in the following result.

For every junction $v \in \mathcal{V}$, and every strictly positive local state vector $\rho^{(v)}$, the maximizing green light policy satisfies

$$h_i^{(v)}(\rho^{(v)}) = \frac{\rho_i}{\sum_{j\in\mathcal{E}_v}\rho_j + \kappa_v}, \quad \forall i \in \mathcal{E}_v\,.$$

Using the explicit expression above allows one to prove the following stability result. The dynamical system (38), with green light policies given by (44), satisfying

$$\sum_{i\in\mathcal{E}_v} \frac{a_i}{C_i} < 1, \quad \forall v \in \mathcal{V}, \tag{46}$$

admits a globally asymptotically stable equilibrium ρ^*, where

$$\rho^{(v)*} = \kappa_v \left(I - \left(\frac{a_i}{C_i} \right)_{i \in \mathcal{E}_v} \mathbf{1}^T \right)^{-1} \left(\frac{a_i}{C_i} \right)_{i \in \mathcal{E}_v}$$

for all $v \in \mathcal{V}$.

We are currently pursuing extensions of our analysis to the multiphase case.

9.4 Comparison Study between Proportionally Fair and Max Pressure Traffic Signal Control Policies for Signalized Arterial Networks

In this section, we present our key results on case studies – further details can be found in our related publication [25].

We first describe the model for traffic flow over arterial networks under signalized intersections. We illustrate some aspects of our model using the 8 intersection sub-network from downtown Los Angeles, which we also use in our simulation studies. This sub-network is shown in Figure 8.

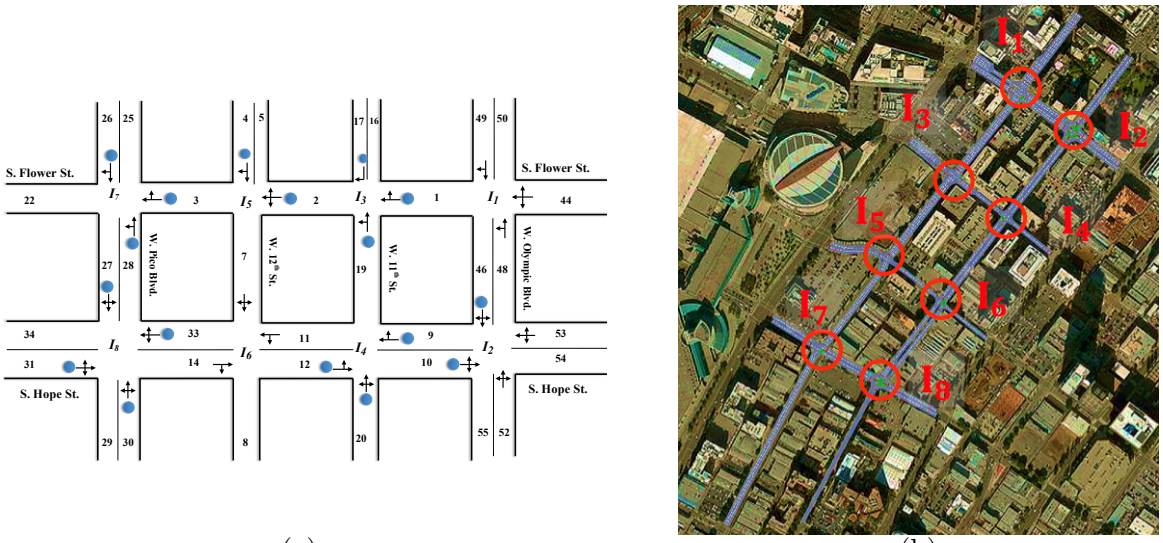

(a) (b)

Figure 8: The Los Angeles downtown sub-network used in the studies: (a) schematic representation, with the solid disks showing the approximate location of loop detector sensors from which we have access to offline traffic count data; (b) aerial view.

An arterial network consists of intersections and links, where a link consists of multiple lanes. We now formulate dynamics that represent mass balance equations for queue lengths associated with different movements. We remark that our purpose is to represent traffic dynamics only to provide context for traffic signal control design. In particular, the controllers presented in this report are evaluated in a microscopic traffic simulator, and not by simulating the dynamics that we present here. The cycle time and offset at every intersection is assumed to be fixed. Their values are described at appropriate places in the report. We describe dynamics for one sample intersection, referring to Figure 9 to illustrate the key concepts.

A *movement* at the intersection is denoted by (i, j) corresponding to an admissible maneuver from the upstream link i into the downstream link j at the intersection. Every link i is divided

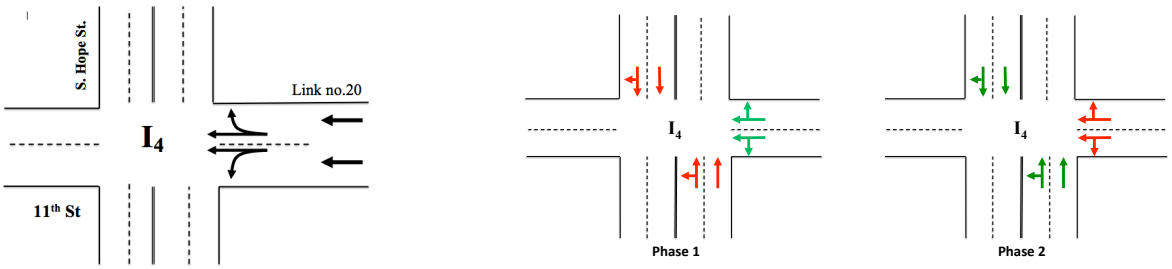

(a) (b)

Figure 9: (a) Illustration of a movement, lane and a link at a sample intersection. Link number 20 contains two lanes, and each lane supports multiple movements. (b) Phase architecture at a sample intersection.

into multiple lanes. A lane can support multiple movements, and the same movement can be made through multiple lanes. Every movement (i, j) is associated with a *saturated flow capacity*, denoted by C_{ij} and a turning ratio β_{ij} denoting the fraction of flow entering link i from upstream and from external to the network, that intends to perform the movement (i, j) and hence the corresponding traffic will queue up in any of the lanes on link i supporting that movement.

The saturated flow capacities for a movement are cumulative over all the lanes which facilitate that movement. The β_{ij} are also referred to as *turning ratios*, and naturally satisfy $\sum_j \beta_{ij} \leq 1$, where the summation is over all movements possible from link i, and the residual $1 - \sum_j \beta_{ij}$ represents the fraction of flow that departs the network from link i. Let the set of phases at the intersection be fixed, and denoted by $\{\phi_1, \ldots, \phi_m\}$. Each phase is associated with, possibly multiple, non-conflicting movements that become active when the phase is given green. At most one phase is given green at any time. We assume that the sub-network used in the simulations satisfies the following:

(P1) Every movement belongs to one and only one phase.

While we impose (P1) for simplicity, it is not difficult to extend the descriptions of the controllers to the settings where (P1) is not satisfied.

Let G be the total green time, i.e., cycle time minus the time for all red and yellow. At the beginning of every cycle, the traffic signal controller updates allocation of green light to every phase. Let the fraction of green time G allocated to phase ϕ_i during the t-th cycle be denoted by $h_\phi[t]$. Let $x_{ij}[t]$ be the number of vehicles waiting in queue to perform the (i, j) movement at the beginning of the t-th cycle, and let $A_i[t]$ be the number of vehicles entering link i from outside the network during the t-th cycle. The dynamics is then given by:

$$x_{ij}[t+1] = x_{ij}[t] + \beta_{ij}\left(A_i[t] + \sum_\ell f_{\ell i}[t]\right) - f_{ij}[t] \tag{47}$$

where $f_{ij}[t]$ is the maximum number of vehicles that can execute (i, j) movement during the t-th cycle, i.e.,

$$f_{ij}[t] = GC_{ij}h_\phi[t],$$

where ϕ is the phase under which (i, j) is activated. We implicitly assume that, if the right hand side of (47) is negative, then it is reset to zero. This would correspond to emptying of the corresponding queue. We clarify that we make this assumption only to simplify the expression for the dynamics

in (47), and also to simplify the design of controllers. However, the microscopic traffic simulations, from which we report results in this section, naturally possess this feature, and hence do not require such an assumption.

We consider decentralized dynamic traffic signal controllers that measure the instantaneous queue lengths in the immediate vicinity of the intersection at the beginning of each cycle to update the green time allocations.[3] Ideally, many existing decentralized controllers, some of which we describe in the next section, require queue length measurements for individual movements. This may be impractical, especially when lanes can support multiple movements. Fortunately, the following features, which are satisfied by real networks, allow us to implement our proposed PF controllers using only queue length measurements for individual lanes. These features also allow intuitive extensions of existing MP controllers which we use for comparison purposes.

(P2) All the movements associated with a given lane are activated in the same phase.

(P2') All the movements associated with a given link are activated in the same phase.

(P2') implies (P2). (P2) is expected to be true for every network. The sub-network used in our simulations satisfies (P2').

Max Pressure (MP) Controller: The MP controller involves adding up *pressures* associated with movements constituting a phase, and then allocating green times as a function of the pressure associated with different phases. The pressure associated with a movement (i, j) at the beginning of the t-th cycle is computed as

$$p_{ij}[t] = C_{ij}\left(x_{ij}[t] - \sum_{\ell} \beta_{j\ell} x_{j\ell}[t]\right), \tag{48}$$

where the summation in ℓ is over all the movements from the downstream link j. The pressure associated with a phase ϕ is the sum of the pressures associated with the movements constituting the phase:

$$p_{\phi}[t] = \sum_{(i,j)\in\phi} p_{ij}[t]. \tag{49}$$

Finally, the green time allocation under MP controller is given by:

$$h^{\mathrm{MP}}_{\phi_r}[t] = \frac{\exp(\eta p_{\phi_r}[t])}{\sum_{s=1}^{m} \exp(\eta p_{\phi_s}[t])} \quad r = 1, \ldots, m\,, \tag{50}$$

where $\eta > 0$ is a parameter to be tuned. When the pressure computation in (48) takes only the non-negative part of the right hand side, when each phase consists of only movement, and when η is very large was originally proposed for communication networks in [8] and extended to traffic signal control in [10]. Since then various extensions have been proposed, e.g., see [11].

Since it is impractical to have queue length measurements for every movement, as would be required to implement (48), we use the following approximation to relate queue lengths for movements and links: $x_{ij}[t] = \beta_{ij} x_i[t]$. This approximation is made only for the purpose of designing appropriate controllers. In particular, the underlying model in the traffic simulation results does

[3] One could consider several variations on queue length measurements, including measurements averaged over previous cycle, which our simulation setup is also equipped to handle. We plan to study the effect of such variations on the resulting traffic dynamics in our future work.

not make any such approximation. The link queue lengths can be readily measured, e.g., in the traffic simulator that we use for our simulation studies. Under the approximation, the pressure associated with a movement can be expressed in terms of link queue lengths as:

$$p_{ij}[t] = C_{ij}\left(\beta_{ij}x_i[t] - \sum_{\ell}\beta_{j\ell}^2 x_j[t]\right). \tag{51}$$

We will denote the MP controller given by (51), (49) and (50) as h^{MP1}. The following approximation has also been proposed, e.g., in [26], to compute the pressure associated with a movement in terms of link queue lengths as:

$$p_{ij}[t] = C_{ij}\left(x_i[t] - x_j[t]\right). \tag{52}$$

We will denote the MP controller given by (52), (49) and (50) as h^{MP2}. An another advantage of (52) is that it does not require information about turning ratios.

An another approach to compute pressure using aggregate link queue length, under (P2'), is proposed in [11] as:

$$p_{\phi}[t] = \sum_{i:\,(i,j)\in\phi} C_i\left(x_i[t] - \sum_{j}\beta_{ij}x_j[t]\right), \tag{53}$$

where $C_i := \sum_j C_{ij}$ is the aggregate saturated flow capacity of all movements associated with link i. We will denote the MP controller given by (53) and (50) as h^{MP3}. A few other variants of MP controllers have been proposed recently, including explicit consideration for lane capacities, e.g., see [27, 28], and replacing turning ratios with their online estimates, e.g., see [11]. One can also write an approximation similar to (51) to compute pressure for a movement in terms of lane queue length measurements. Such an approximation will be relevant, e.g., when the network satisfies the weaker property of (P2).

While MP controllers have attracted considerable attention in the recent past, the PF controllers, which we describe next, have received very little attention.

Proportionally Fair (PF) Controller: The implementation of the PF controller requires, for every phase, aggregate queue length over all the movements associated with the phase. This is the same as the total queue length over all the lanes (or links) activated by a phase under (P2) (or (P2')). Let $x_{\phi}[t]$ be the aggregate queue length associated with phase ϕ at the beginning of the t-th cycle. The green time allocation under PF controller $h^{\mathrm{PF}}[t]$ is equal to the value of θ corresponding to the optimal solution of the following:

$$\begin{aligned} \text{maximize} \quad & \sum_{r=1}^{m} x_{\phi_r}[t]\log\theta_r \\ \text{subject to} \quad & \theta_r \geq 0, \quad r = 1,\ldots,m \\ & \sum_{r=1}^{m}\theta_r = 1 \end{aligned} \tag{54}$$

When (P1) is satisfied, the solution to (54) can be written in closed form as follows:

$$h_{\phi_r}^{\mathrm{PF}}[t] = \frac{x_{\phi_r}[t]}{\sum_{s=1}^{m} x_{\phi_s}[t]}, \quad r = 1,\ldots,m$$

This means that the green time allocated to a phase ϕ_r under PF policy is proportional to the aggregate queue length associated with ϕ_r. We choose to write (54) in its current form because it can be readily adapted to settings where (P1) is not satisfied, e.g., see our recent work [24] for details. In fact, the control implementation in VISSIM described in the Simulations section implements the PF controller for the general setting, for which the optimization in eq. (54) is convex, and can be solved in real-time using available software tools such as `cvx` [6, 7].

Simulations: The road network shown in Figure 8 a) is created in PTV VISSIM while respecting appropriate geometric proportions, using Google Maps and signal timing charts procured from LADoT. We used arterial loop detector data collected from May 9 to May 31, 2013 at the locations shown in Figure 8 (a) to extract the arrival rates. The data included volume, speed and occupancy, recorded once every 5 minutes. External arrival rate for each incoming link is set to the mean value between 5-7 pm. The resulting arrival rates are as follows (all in veh / hour):

$$\lambda_{17} = 231,\ \lambda_4 = 156,\ \lambda_{26} = 45,\ \lambda_{31} = 30,\ \lambda_{30} = 79,\ \lambda_{20} = 240, \tag{55}$$

$\lambda_{44}, \lambda_{49}, \lambda_{52}, \lambda_{53}$ were missing in the data set and they all are set to 200 veh/hour.

The saturated flow capacities are measured offline in VISSIM for every movement. The saturated flow capacity is 2200 vehicle/hour/lane for through movement and 1800 vehicle/hour/lane for right-turn and left-turn movements. These values are relatively close to the standard values reported in HCM 2000 [29]. Turn ratios are assumed to be equally distributed between the admissible movements at incoming link of each intersection. The values of cycle time and total green light time per cycle for each intersection are obtained from LADoT signal timing charts. The green light time and cycle time for all the intersections are 80 seconds and 90 seconds respectively. We consider two scenarios for the simulations: zero offset and non-zero offset. For the non-zero offset scenario, we use the offsets from LADoT timing chart. The signal offsets are 77, 73, 47, 77, 15, 27, 64, and 36 seconds for intersections $I1$ to $I8$ respectively.

All the simulation runs were started with an empty network, and, referring to (50), we used $\eta = 0.1$ in all our MP controller implementations. Every intersection has two phases: one corresponding to north south movements, and the other one for the east west movements, as shown in Figure 9(b) for a sample intersection. The overall architecture for interfacing our control implementation with VISSIM simulator is shown in Figure 10.

We report comparison between MP1, MP2, MP3 and PF controllers with respect to network throughput and average travel time.

The network throughput is described in terms of *feasible* external inflows. A set of external inflows λ is said to be feasible for a given network under given turning ratios β, saturated flow capacities C, and a control policy if the fraction of vehicles spilling outside the boundary of the network is negligible. Since there are 10 entry points in our network, the set of feasible external inflows is a 10 dimensional set. In general, it is hard to compute this set exactly. We first describe a simple procedure to compute an outer approximation to this set. Let $z(\lambda, \beta, C)$ be the corresponding vector of steady-state flows under fixed-time controllers associated with various movements. Then a necessary condition for the external inflow λ to be feasible is that the corresponding steady-state flow satisfies the following at every intersection.

$$\sum_{r=1}^{m} \max_{(i,j)\in\phi_r} \frac{z_{ij}}{C_{ij}} \leq \frac{G}{T}, \tag{56}$$

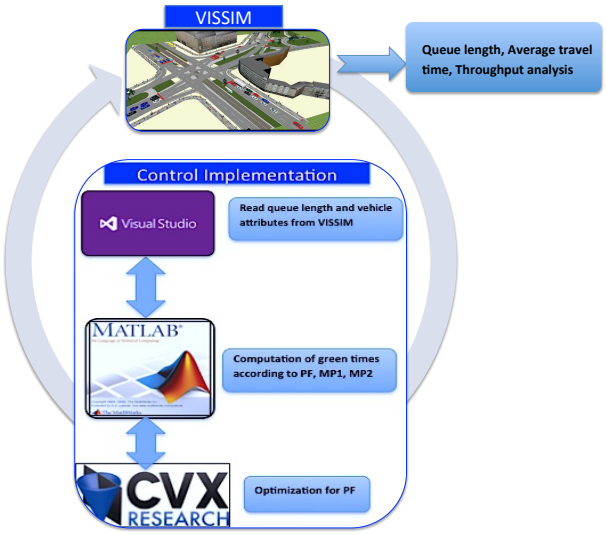

Figure 10: An overview of the implementation of control architecture with VISSIM.

i.e., the sum of the critical flow ratio associated with different phases, at every intersection, is less than the ratio of green light time to total cycle time. Such a condition is standard for fixed time controllers.

We compared the outer approximation with simulations in VISSIM for various control policies. For every control policy, we start with nominal external inflows in (55), and then increase one component until the fraction of vehicles spilling outside the network at each of the 10 entry points is less than 5 %. The maximum value is reported in Table 4 for each of the three control policies for a few representative components. These results suggest that in both zero offset and non-zero offset scenarios, the throughput of PF controller is comparable to the MP1 controller, and significantly better than the MP2 and MP3 controllers proposed in the literature.

		PF		MP1		MP2		MP3	
$\lambda_i^{\max}$	Upper bound	Zero offset	Non-zero offset	Zero offset	Non-zero offset	Zero offset	Non-zero offset	Zero offset	Non-zero offset
i=4	3140	2500-2600	2100-2200	2300-2400	2400-2500	2000-2100	1200-1300	1900-2000	1300-1400
i=26	4310	2600-2700	2800-2900	2500-2600	2500-2600	1500-1600	1400-1500	1600-1700	1400-1500
i=30	4510	2800-2900	2800-2900	2900-3000	2800-2900	1900-2000	1600-1700	1800-1900	1800-1900

Table 4: Comparison of the upper bound on network throughput capacity as given by the outer approximation in (56), and the the ones found through simulation studies under PF, MP1, MP2 and MP3 controllers. Each row gives the maximum feasible external inflow, in vehicles per hour, at the corresponding entry point of the network, when the arrival rates at all other entry points are fixed at their nominal values given by (55).

We computed the travel time under the three control policies, for external inflow equal to 4 times the nominal values given in (55). This external inflow was first checked to be feasible, and was chosen so as to simulate *heavy traffic*, i.e., traffic conditions which are barely feasible [4]. We borrow the *heavy traffic* terminology from the queueing theory literature. The output file from

[4]While we evaluate travel times under various controllers for feasible demands, the controllers as such are applicable even for infeasible demands. A thorough comparison of performances between various controllers under infeasible demands, and the corresponding implication for controller design is left for future work.

VISSIM gives, for every simulation instant, the time spent by every vehicle currently present in the network up to that time instant. This data is used to compute the running average of the travel time for all the vehicles, including the ones which have departed the network. Figure 11 shows the average travel time based on 5 stochastic simulation runs in VISSIM. The confidence intervals of the results are shown by the error bars. Each error bar represents one standard deviation on either side of the mean.

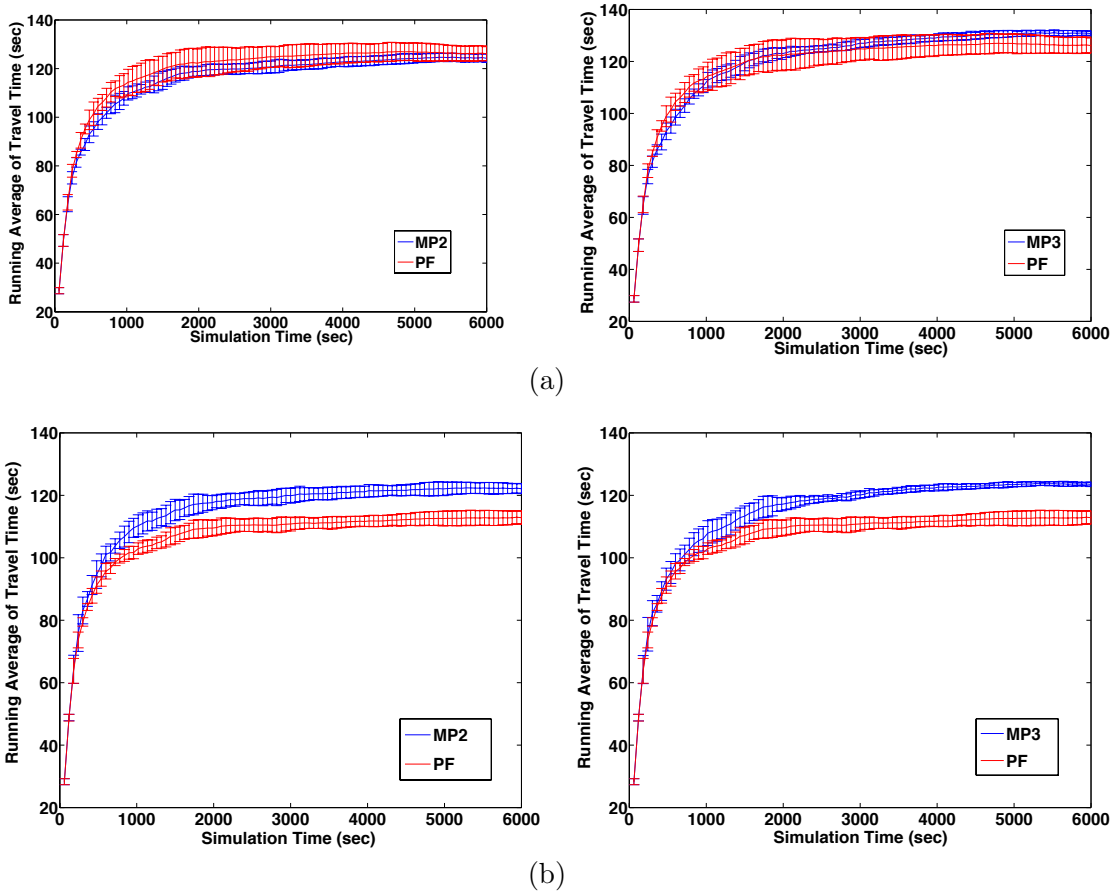

Figure 11: Comparison of the running average of travel time for heavy traffic under PF and MP controllers using (a) Zero offset and (b) Non-zero offset.

Figure 11 shows that, in non-zero offset scenario, the average travel time under PF is consistently better than the MP2 and MP3 controllers, and, for the zero offset scenario, the performance of PF controllers is comparable to its MP counterparts in spite of its minimalistic nature.

Table 5 shows that for zero offset scenario, with some exceptions, steady state queue lengths are lower under PF in comparison to MP controllers. The links which show the reverse trend (e.g., link 10) are typically the ones whose *dominant* movement has a downstream link exiting the network. On the other hand, e.g., link 1 also has a movement (right turning) which exits the network, but this movement is not dominant because it shares only one lane with through movement, whereas the through movement has 3 dedicated lanes, and is not exiting. For the non-zero offset scenario, the queue lengths under PF policy are comparable to the ones under MP1 and

are lower than MP2 and MP3 on most links. We recall that, for the purpose of computation of pressure in our implementation of MP controllers, we assume zero queue length on the exit lengths, and hence the links with dominant movement exiting the network has a relatively high pressure in comparison to the other links at that intersection whose dominant movements do not exit the network. This feature highlights the *boundary effect* on the queue lengths under MP controllers. The PF controllers, however do not exhibit such a boundary effect because the green time allocation is determined based on queue length measurements only on links at that intersection.

Link No.	1	2	3	4	7	9	10	11	12	19	20	28	33	44	46	48	49	52	53
PF	5.11	21.38	5.55	4.66	7.32	5.43	15.46	6.43	15.03	2.85	6.15	4.84	3.26	3.26	2.68	5.66	5.61	3.19	14.45
MP1	12.47	25.18	9.78	6.33	3.09	9.09	6.31	9.10	6.19	4.82	10.48	2.03	5.06	7.20	5.58	7.08	6.48	9.41	10.45
MP2	12.69	18.15	11.30	6.73	8.53	9.21	6.27	11.10	5.01	4.17	10.21	3.44	5.64	7.07	10.34	9.91	7.44	8.79	9.29
MP3	10.95	29.25	8.88	6.21	7.59	10.83	5.99	9.31	4.33	6.44	9.78	2.33	4.73	6.67	13.61	9.43	7.77	8.35	10.12

(a)

Link No.	1	2	3	4	7	9	10	11	12	19	20	28	33	44	46	48	49	52	53
PF	11.27	16.07	10.03	4.48	5.45	8.20	5.41	9.66	4.41	3.72	10.87	3.57	6.12	7.70	11.33	5.67	5.23	18.95	7.71
MP1	11.85	17.12	10.97	4.79	5.54	8.48	6.37	8.06	3.45	4.31	11.31	3.22	5.90	9.08	9.70	5.20	5.06	10.27	7.77
MP2	13.44	19.67	9.89	6.06	4.86	9.95	5.63	8.94	4.57	2.74	10.30	3.11	6.53	6.91	12.65	9.97	7.73	8.29	10.79
MP3	9.96	13.44	11.05	9.27	9	11.42	5.03	10.73	5.35	5.56	10.53	2.78	5.21	6.05	10.85	10.79	7.46	10.99	10.36

(b)

Table 5: Comparison of steady state average queue lengths on representative links under various control policies using (a) Zero offset (b) Non-zero offset. Refer to Figure 8 (a) for link number identifiers. For brevity, queue lengths are reported only for those links which show significant difference across the three control policies.

The feature of the MP controllers to allocate green time based on comparison between upstream and downstream queue lengths gives rise to *phase shift* in the queue length profiles between adjacent links of the network, as illustrated in Figure 12 and 13. Indeed, this phase shift builds the necessary pressure to extract green time for the upstream link (link no. 44 in Figure 12). The queue lengths under PF controller, however are decoupled, and do not show a phase shift. Figure 13 shows that the phase shift behavior changes in non-zero offset scenario compare to the zero offset scenario. However, even in non-zero offset scenario, the MP controller shows larger phase shift in comparison to PF controller. This phase shift might be responsible for higher average queue lengths under MP controllers in comparison to PF controller.

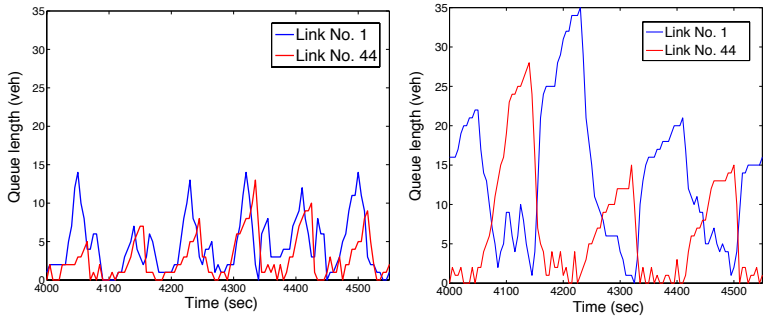

(a) (b)

Figure 12: Illustration of phase shift in queue length time series on link numbers 1 and 44, which are adjacent to each other (see Figure 8(a)), under (a) PF and (b) MP2 controllers under zero offset.

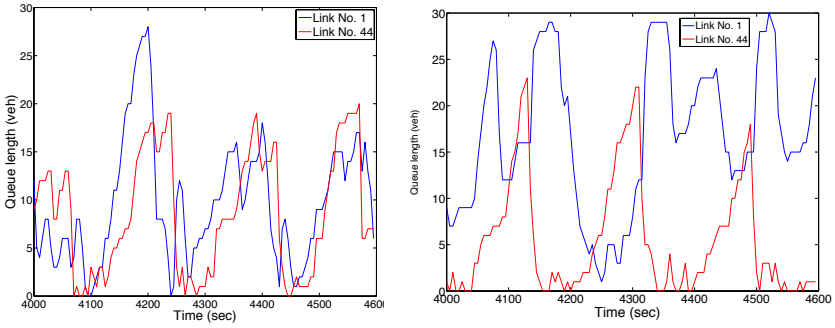

(a) (b)

Figure 13: Illustration of phase shift in queue length time series on link numbers 1 and 44, which are adjacent to each other (see Figure 8(a)), under (a) PF and (b) MP2 controllers under non-zero offset

10 Conclusions and Recommendations

Our major findings and conclusions are as follows:

1. For the system optimum dynamic traffic assignment, we proposed a relaxation of realistic traffic dynamics, wherein the total inflow into and total outflow from the cells are independently upper-bounded by supply and demand respectively. We also design open-loop variable speed, ramp metering and routing controllers that ensure feasibility of the optimal solutions under relaxed constraints with respect to several realistic traffic dynamics modeled by a combination of cell-based features of the Cell Transmission Model and general Dynamic Network Loading Model that includes FIFO and non-FIFO policies. We also derive bounds on perturbations in the system trajectory under the proposed open loop controllers, with respect to perturbations in initial condition and external inflow. These results significantly expand the known results in terms of relationship between computationally efficient SO-DTA formulations and the feasibility of their optimal solutions with respect to realistic traffic dynamics.

2. The convexity of the equilibrium selection problem and the distributedness of the underlying traffic dynamics allowed us to adapt two well-known optimization methods to develop algorithms that compute optimal solutions to the equilibrium selection problem in a distributed manner.

3. We studied stability of some minimalist decentralized traffic signal control policies for urban traffic networks. Our main theoretical result shows that, in the case when only single phases are allowed, the resulting traffic network dynamics admit a globally asymptotically stable equilibrium, provided that the arrival rates belong to the interior of a certain stability polytope. These results rely on the use of some entropy-like Lyapunov functions previously considered in the context of stochastic queuing networks. Our ongoing studies suggest that these favorable properties also extend to several complex phase architectures.

4. We presented a unified framework to distinguish between several variants of max pressure (MP) controllers in terms of the granularity of real-time queue length measurements required for their implementation. Proportionally fair (PF) controller does not require information

about turning ratios, saturated flow capacities and downstream queue length in comparison to the majority of its MP counterparts. In spite of this minimalist nature, in our microscopic simulation studies on a Los Angeles downtown sub-network in PTV VISSIM, PF controllers outperforms MP controllers in terms of throughput and average delay time in non-zero offset scenario. In the zero offset scenario, the performance of PF controller is comparable to its MP counterparts. The feature of the MP controllers to allocate green time based on comparison between upstream and downstream queue lengths gives rise to *phase shift* in the queue length profiles between adjacent links of the network. Indeed, this phase shift builds the necessary pressure to extract green time for the upstream link. The queue lengths under PF controller, however are decoupled, and do not show a phase shift. The phase shift behavior changes in non-zero offset scenario compare to the zero offset scenario. However, even in non-zero offset scenario, the MP controller shows larger phase shift in comparison to the PF controller. This phase shift might be responsible for higher average queue lengths under MP controllers in comparison to the PF controller.

11 Deployment and Implementation

No data was gathered in this project. No deployment or implementation were done in this project.

12 Appendices

Not Applicable.

13 References

References

[1] D.K. Merchant and G.L. Nemhauser. A model and an algorithm for the dynamic traffic assignment problem. *Transportation Science*, 12:183–199, 1978.

[2] D.K. Merchant and G.L. Nemhauser. Optimality conditions for a dynamic traffic assignment model. *Transportation Science*, 12:200–207, 1978.

[3] Srinivas Peeta and Athanasios K Ziliaskopoulos. Foundations of dynamic traffic assignment: The past, the present and the future. *Networks and Spatial Economics*, 1(3-4):233–265, 2001.

[4] Carlos F Daganzo. The cell transmission model: A dynamic representation of highway traffic consistent with the hydrodynamic theory. *Transportation Research Part B: Methodological*, 28(4):269–287, 1994.

[5] A. Muralidharan and R. Horowitz. Optimal control of freeway networks based on the link node cell transmission model. In *Proceedings of the American Control Conference (ACC)*, pages 5769–5774, June 2012.

[6] Inc. CVX Research. CVX: Matlab software for disciplined convex programming, version 2.0. `http://cvxr.com/cvx`, August 2012.

[7] M. Grant and S. Boyd. Graph implementations for nonsmooth convex programs. In V. Blondel, S. Boyd, and H. Kimura, editors, *Recent Advances in Learning and Control*, Lecture Notes in Control and Information Sciences, pages 95–110. Springer-Verlag Limited, 2008.

[8] Leandros Tassiulas and Anthony Ephremides. Stability properties of constrained queueing systems and scheduling policies for maximum throughput in multihop radio networks. *Automatic Control, IEEE Transactions on*, 37(12):1936–1948, 1992.

[9] T. Wongpiromsarn, T. Uthaicharoenpong, Y. Wang, E. Frazzoli, and D. Wang. Distributed traffic signal control for maximum network throughput. In *IEEE Conference on Intelligent Transportation Systems*, pages 588–595, Anchorage, AK, 2012.

[10] Pravin Varaiya. The max-pressure controller for arbitrary networks of signalized intersections. In *Advances in Dynamic Network Modeling in Complex Transportation Systems*, pages 27–66. Springer, 2013.

[11] Tung Le, Péter Kovács, Neil Walton, Hai L Vu, Lachlan LH Andrew, and Serge SP Hoogendoorn. Decentralized signal control for urban road networks. *Transportation Research Part C: Emerging Technologies*, 2015.

[12] R. K. Ahuja, T. L. Magnanti, and J. B. Orlin. *Network Flows: Theory, Algorithms, and Applications*. Prentice Hall, 1993.

[13] Michael J Lighthill and Gerald Beresford Whitham. On kinematic waves. ii. a theory of traffic flow on long crowded roads. *Proceedings of the Royal Society of London. Series A. Mathematical and Physical Sciences*, 229(1178):317–345, 1955.

[14] Carlos F Daganzo. The cell transmission model, part ii: network traffic. *Transportation Research Part B: Methodological*, 29(2):79–93, 1995.

[15] Athanasios K Ziliaskopoulos. A linear programming model for the single destination system optimum dynamic traffic assignment problem. *Transportation science*, 34(1):37–49, 2000.

[16] A. Hegyi, B. De Schutter, and H. Hellendoorn. Model predictive control for optimal coordination of ramp metering and variable speed limits. *Transportation Research Part C*, 13(3):185 – 209, 2005.

[17] E. Cascetta. *Transportation Systems Analysis*. Springer, 2009.

[18] K. Doan and S.V. Ukkusuri. On the holding-back problem in the cell transmission based dynamic traffic assignment models. *Transportation Research Part B: Methodological*, 46(9):1218 – 1238, 2012.

[19] G. Como, E. Lovisari, and K. Savla. Convexity and robustness of dynamic traffic assignment for control of freeway networks. *Transportation Research Part B: Methodological*, 2015. Under revision. Available at `http://arxiv.org/abs/1509.06189`.

[20] E. Lovisari, G. Como, A. Rantzer, and K. Savla. Stability analysis and control synthesis for dynamical transportation networks. Available at `http://arxiv.org/abs/1410.5956`, 2014.

[21] E. Lovisari, G. Como, and K. Savla. Stability of monotone dynamical flow networks. In *IEEE Conference on Decision and Control*, Los Angeles, CA, 2014.

[22] Michael Zargham, Alejandro Ribeiro, Asuman Ozdaglar, and Ali Jadbabaie. Accelerated dual descent for network flow optimization. *IEEE Trans. Automatic Control*, 59(4):905 – 920, 2014.

[23] Q. Ba, K. Savla, and G. Como. Distributed optimal equilibrium selection for traffic flow over networks (extended version). In *IEEE Conference on Decision and Control*, Osaka, Japan, 2015. Available at `http://www-bcf.usc.edu/∼ksavla/papers/Ba.Savla.ea.DistributedCDC15.pdf`.

[24] G. Nilsson, P. Hosseini, G. Como, and K. Savla. Entropy-like Lyapunov functions for the stability analysis of adaptive traffic signal controls. In *IEEE Conference on Decision and Control*, Osaka, Japan, 2015. Available at `http://www-bcf.usc.edu/∼ksavla/papers/TrafficControl-CDC2015.pdf`.

[25] P. Hosseini and K. Savla. A comparison study between proportionally fair and max pressure controllers for signalized arterial networks. In *Transportation Research Board Annual Meeting*, 2016.

[26] Jean Gregoire, Emilio Frazzoli, Arnaud de La Fortelle, and Tichakorn Wongpiromsarn. Back-pressure traffic signal control with unknown routing rates. In *IFAC World Congress*, 2014.

[27] Anastasios Kouvelas, Jennie Lioris, S Fayazi, and Pravin Varaiya. Maximum pressure controller for stabilizing queues in signalized arterial networks. *Transportation Research Record: Journal of the Transportation Research Board*, (2421):133–141, 2014.

[28] J. Gregoire, X. Qian, E. Frazzoli, A. de La Fortelle, and T. Wongpiromsarn. Capacity-aware back-pressure traffic signal control. *IEEE Transactions on Control of Network Systems*, 2(2):164 – 173, 2015.

[29] Highway Capacity Manual. Hcm 2000. *Washington, DC: Transportation Research Board*, 2000.